Low Cycle Fatigue Behavior of 316LN Stainless Steel Alloyed with Varying Nitrogen Content. Part I: Cyclic Deformation Behavior

G.V. PRASAD REDDY, R. SANDHYA, S. SANKARAN, and M.D. MATHEW

In this study, the influence of cyclic strain amplitude on the evolution of cyclic stress–strain response and the associated cyclic deformation mechanisms in 316LN stainless steel with varying nitrogen content (0.07 to 0.22 wt pct) is reported in the temperature range 773 K to 873 K (500 °C to 600 °C). Two mechanisms, namely dynamic strain aging and secondary cyclic hardening, are found to strongly influence the cyclic stress response. Deformation substructures associated with both the mechanisms showed planar mode of deformation. These mechanisms are observed to be operative over certain combinations of temperature and strain amplitude. For strain amplitudes >0.6 pct, wavy or mixed mode of deformation is noticed to suppress both the mechanisms. Cyclic stress–strain curves revealed both single and dual-slope behavior depending on the test temperature. Increase in nitrogen content is found to increase the tendency toward planar mode of deformation, while increase in strain amplitude leads to transition from planar slip bands to dislocation cell/wall structure formation, irrespective of the nitrogen content in 316LN stainless steel.

DOI: 10.1007/s11661-014-2428-5

I. INTRODUCTION

PRIMARY side components (main vessel, inner vessel, intermediate heat exchanger, *etc*.) of Indian Prototype Fast Breeder Reactor (PFBR) are fabricated from 316LN austenitic stainless steel (SS) containing 0.06 to 0.08 wt pct nitrogen. The section thicknesses of these components reach up to 30 mm. From the perspective of cost and thermal stresses, it is necessary to reduce the section thickness of these components which in turn demands the use of high-strength nitrogen-alloyed 316LN SS with increased resistance to low cycle fatigue (LCF) failure (LCF being one of the design considerations).

Nitrogen addition in austenitic SS is found to induce cyclic softening which has been attributed to the disordering of Cr-N short-range orders (SROs).[1] The interaction of these SROs with dislocations promotes planar slip, in addition to that caused by decrease in stacking fault energy (SFE) due to nitrogen addition.[2] Also, in the present study, cyclic stress–strain response is observed to be strongly influenced by dynamic strain aging (DSA) and secondary cyclic hardening (SCH), which occurred in the investigated temperature range [773 to 873 K (500 °C to 600 °C)] that encompasses the PFBR steady state operating temperature [about 820 K (547 °C)] and temperatures encountered during power transients. DSA causes localized planar slip and high matrix hardening that leads to drastic reduction in LCF life,[3,4] while SCH increases the degree of hardening over and above that caused by DSA.[5] Hence, it is utmost important to study the influence of these underlying phenomena on cyclic deformation behavior of nitrogen-alloyed 316LN SS. Accordingly, LCF tests were conducted to study the combined influence of nitrogen and total strain amplitude, in the temperature range 773 K to 873 K (500 °C to 600 °C), on LCF deformation and life in 316LN SS alloyed with different nitrogen contents of 0.07, 0.11, 0.14, and 0.22 wt pct. Several LCF studies have been conducted previously, on high nitrogen 316LN SS with an emphasis on the effect of nitrogen content on substructural evolution and fatigue life.[6–10] In the present study, the mechanisms that control the LCF deformation, life, and associated substructures are elucidated in a systematic way over a range of test parameters. This study is presented in two parts: part-I deals with the evolution of cyclic deformation behavior (current paper), and part-II details LCF life variation as a function of nitrogen, total strain amplitude, and temperature.[11]

G.V. PRASAD REDDY, Scientific Officer-E, R. SANDHYA, Head Fatigue Studies Section, and M.D. MATHEW, Head, are with the Mechanical Metallurgy Division, Indira Gandhi Center for Atomic Research, Kalpakkam 603102, India. Contact e-mail: prasadreddy@igcar.gov.in, varprasad@gmail.com S. SANKARAN, Associate Professor, is with the Department of Metallurgical & Materials Engineering, Indian Institute of Technology Madras, Chennai 600036, India.

Manuscript submitted January 11, 2014.
Article published online July 9, 2014

II. MATERIAL AND EXPERIMENTAL DETAILS

Four commercial scale heats of 316LN SS, containing 0.07, 0.11, 0.14, and 0.22 wt pct nitrogen (henceforth designated as N07, N11, N14, and N22, respectively) were produced by combination of air induction melting (AIM) and electro slag refining (ESR) processes. The

Table I. Chemical Composition (in Weight Percent) of Nitrogen-Alloyed 316LN Austenitic Stainless Steels

Designation	C	Cr	Ni	Mo	N	Mn	S	P
N07	0.03	17.5	12.2	2.49	0.07	1.7	0.0055	0.013
N11	0.03	17.6	12.2	2.51	0.11	1.78	0.0055	0.015
N14	0.03	17.5	12.1	2.53	0.14	1.74	0.0041	0.017
N22	0.03	17.5	12.3	2.54	0.22	1.7	0.0055	0.018

carbon content in all heats was maintained at around 0.03 wt pct. The amount of all the other elements was kept unchanged in all heats. The ESR ingots were hot forged to slabs which were then hot rolled into plates of 22-mm thickness. The chemical composition of the four heats of 316LN SS is given in Table I. Rectangular blanks of 115 × 24 × 22 mm dimension, cut from the rolled plates in the rolling direction, were solution annealed at 1363 K (1090 °C) for 60 minutes followed by water quenching. Equiaxed grains free of precipitates and delta-ferrite have been observed, and the average grain size of four heats, measured through mean intercept method, lies within the 89 ± 13 μm, as per the histogram shown in Figure 1(a) for N07, N14, and N22 (N11 is not shown in Figure 1(a) for clarity). Specimens with 25-mm cylindrical gage length and 10-mm gage diameter were used for the LCF tests conducted in strain control mode, in the temperature range of 773 K to 873 K (500 °C to 600 °C) with total strain amplitudes of ±0.25, 0.4, 0.6, 0.8, and 1.0 pct at 3×10^{-3} s^{-1} strain rate. Also LCF test at 0.6 pct strain amplitude was conducted at 300 K (27 °C), for all the 316LN SS heats. For transmission electron microscopy (TEM) studies, thin foils were prepared from the region close to the fractured section of the tested specimens. 10 pct perchloric acid in methanol (in 1:9 ratio) was used as electrolyte for twin-jet thinning. The foils were examined with 120 kV TEM (CM 12 Philips). Dislocation structures in the heat-treated samples consisted of randomly distributed dislocations and stacking faults with partial dislocations at all the nitrogen contents, as shown in Figure 1(b). In addition to these, 316LN SS with 0.14 and 0.22 wt pct N is found to consist of dislocation pairs (Figure 1(c)).

III. RESULTS AND DISCUSSION

A. *Factors/Phenomena Influencing Cyclic Deformation Behavior*

Cyclic deformation behavior of nitrogen-alloyed 316LN SS is influenced, in general, by interstitial nitrogen, SFE, SROs, DSA, and SCH depending on the test temperature and applied strain amplitude. Hence, in the following text, LCF deformation is first discussed at 300 K (27 °C) and then at high temperatures. Cyclic deformation behavior is described in the present study in terms of cyclic stress response (CSR) curves and the deformation substructures. CSR curves exhibited regions of initial cyclic hardening followed by cyclic softening and/or cyclic saturation before the rapid stress drop associated with macrocrack propagation. In addition to the above 3 or 4-stage CSR, SCH, *i.e.*, hardening after stabilization, is noticed for all the steels before failure. The occurrence and also the extent of these regions are found to be strongly dependent on applied strain amplitude and test temperature.

1. *Role of interstitial nitrogen, SROs, and stacking fault energy on strengthening and planar slip*

Figure 2(a) illustrates the influence of nitrogen content on CSR for the LCF tests at ±0.6 pct strain amplitude and 300 K (27 °C) test temperature. Cyclic strengthening by nitrogen addition can be noticed from Figure 2(a). The probable reasons for this nitrogen-induced cyclic strengthening are briefed below. Interstitial strengthening by nitrogen alone is nominal as nitrogen introduces cubic elastic distortions that do not interact with screw dislocations and show a weak interaction with edge dislocations, in face-centered cubic lattice. Nonetheless, electrostatic interaction between negatively charged nitrogen atoms and positively charged dislocations is reported to result in effective pinning of dislocations by nitrogen atoms.[12] In addition, distribution of nitrogen atoms in the Cr-N short-range order provides an additional strengthening to the nitrogen-alloyed 316LN SS.[12] These interstitial-substitutional SROs cause non-cubic distortions and hence contribute to strong interaction with dislocations in austenitic steels.[12,13] Hence, strengthening in nitrogen-alloyed 316LN SS is attributed to the above mentioned mechanisms, based on the fundamental deformation studies.[12–14]

316LN SS is essentially a planar slip material tendency to which can be increased further, by reducing SFE with nitrogen addition[8] and also by the presence of Cr-N SROs in 316LN SS.[2,8] For the range of nitrogen content used in the present study, change in SFE is reported to vary in the range of 15 to 28 mJ/m^2 with change in nitrogen from 0.03 to 0.25 wt pct in 316L SS.[8,15] Hence, the source of planar slip in nitrogen-alloyed 316LN SS, in this study, is primarily attributed to the SROs and reduction in SFE. It is shown that SROs assist planar slip, because each successive dislocation requires a lower stress to pass over the slip plane as compared to the first one which passes through the ordered crystal and consumes additional energy to shift the atoms from low energy sites.[12] This implies that SROs should induce cyclic softening *i.e.*, gradual stress decrease during strain cycling. Interestingly, this has been noticed in the room temperature CSR curves shown in Figure 2(a). As apparent from Figure 2(a), after the brief initial cyclic hardening up to the peak stress, the amount of softening increased with increase in nitrogen content particularly for N14 and N22 steels at

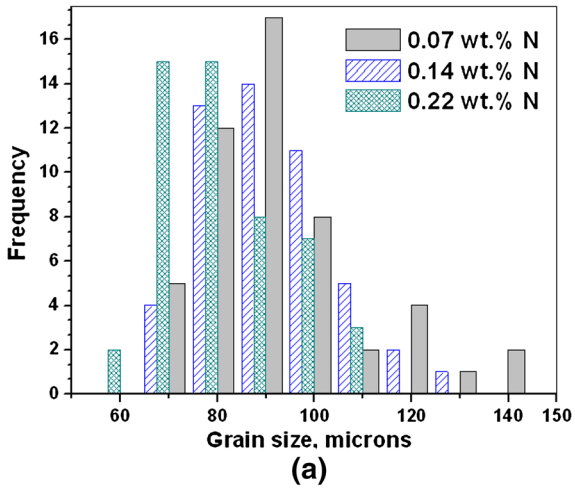

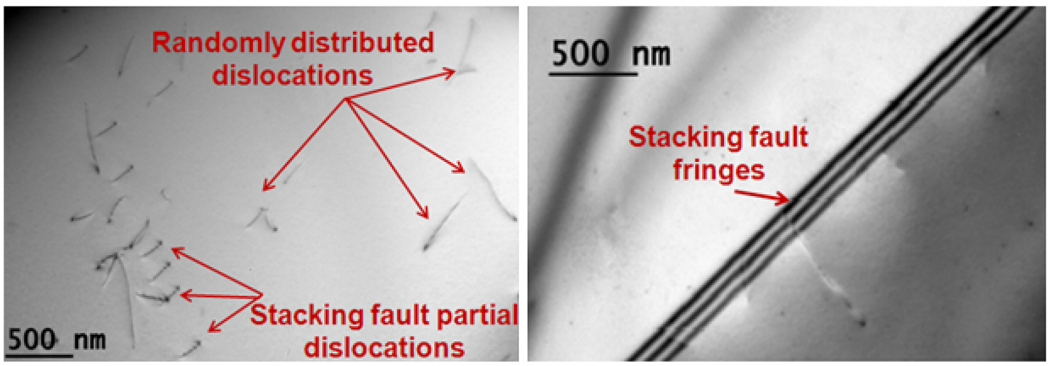

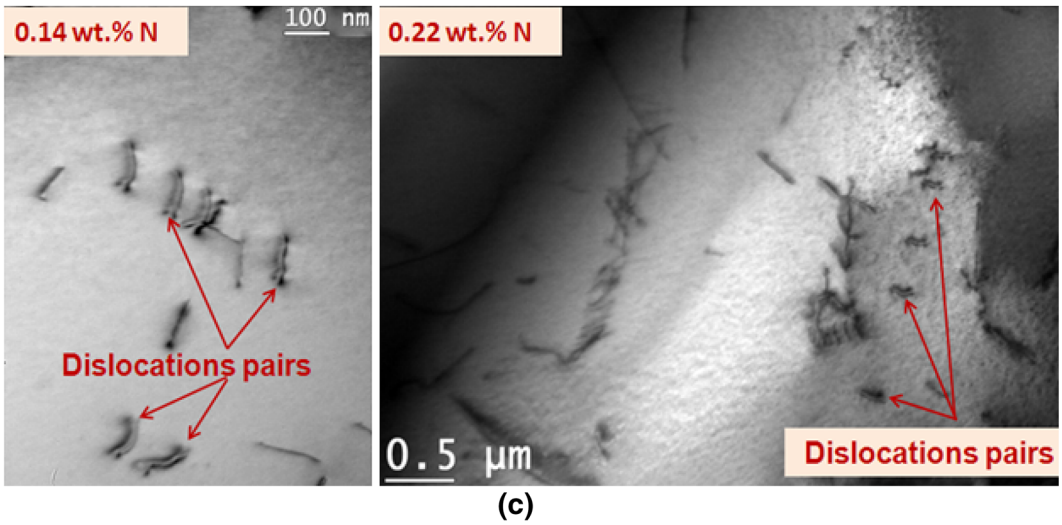

Fig. 1—(*a*) Histogram plots of grain size variation as a function of nitrogen content in 316LN stainless steels; (*b*, *c*) Bright field TEM images of dislocation structure in heat-treated and untested samples of 316LN SS: (b) Random distribution of dislocations and stacking faults, and (c) Dislocation pairs (observed in 316LN SS with 0.14 and 0.22 wt pct N).

300 K (27 °C). The magnitude of the amount of softening at 300 K (27 °C), shown in Figure 2(b), unambiguously signifies the fact that nitrogen addition induces cyclic softening; the amount of softening is calculated as the difference between peak stress and half-life stress. This indirectly indicates that the presence of SROs and its identity has been revealed as Cr-N and/or Mo-N SROs by techniques such as Atom Probe Field Ion Microscope,[16,17] Neutron Spectroscopy,[18] and combined XANES and EXAFS[1] in FeCrNi/FeCrNiMo/FeCr austenitic/duplex stainless steels. Even though higher nitrogen contents promote cyclic softening (Figure 2(b)), cyclic stress throughout the cycling remained over and above that of low nitrogen

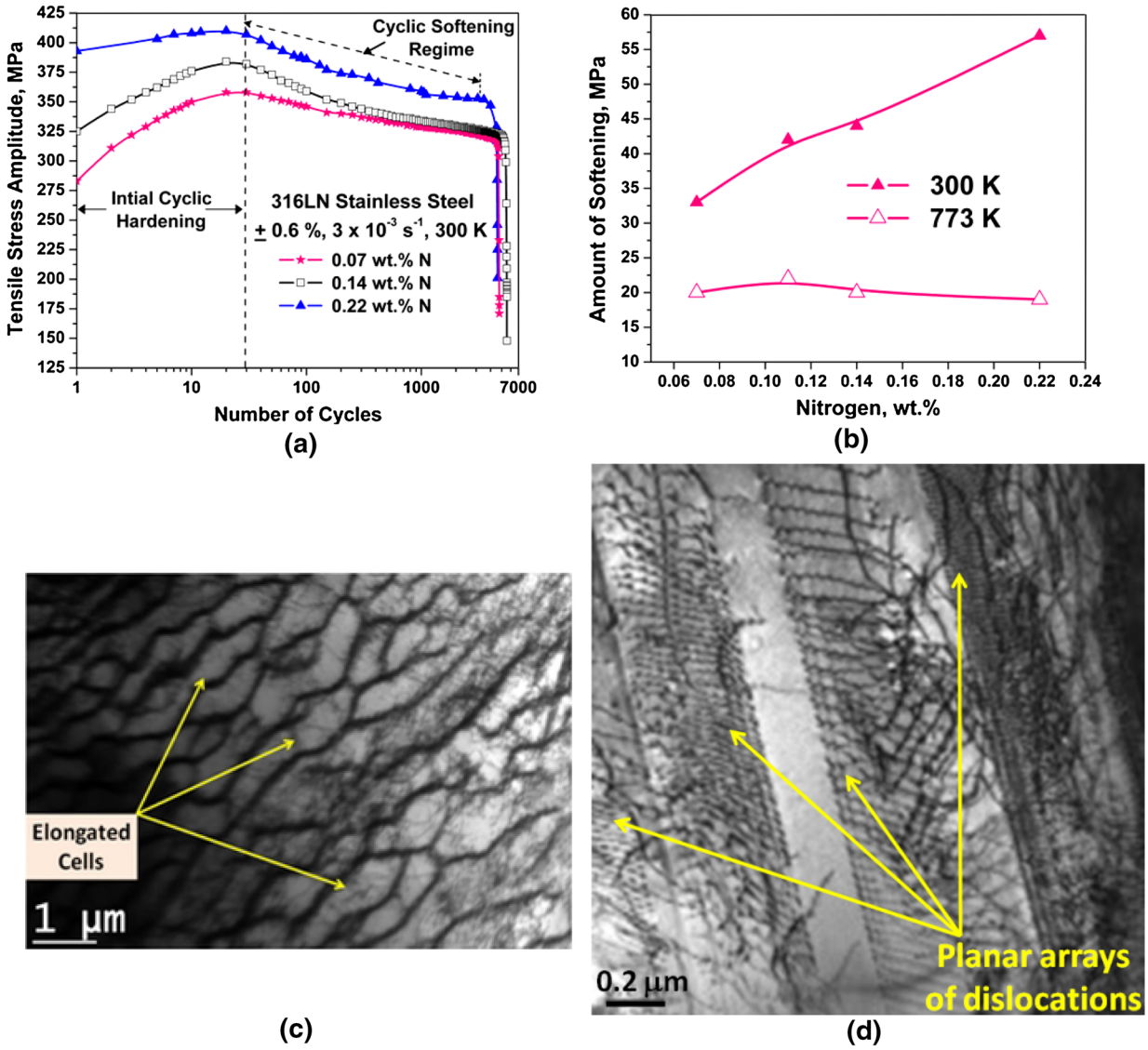

Fig. 2—(*a*) Cyclic stress response (CSR) curves at 300 K (27 °C) and 0.6 pct amplitude for N07, N14, and N22 steels, (*b*) Comparison of amount of cyclic softening (*i.e.*, difference in peak stress and half-life stress in CSR curves) between 300 K (27 °C) and 773 K (500 °C) at 0.6 pct strain amplitude, as a function of nitrogen content, (*c*, *d*) Cyclic deformation substructure at 300 K (27 °C) and 0.6 pct amplitude for (c) N07 and (d) N22 steels.

counterparts (Figure 2(a)). The presence and destruction of such SROs during LCF deformation and subsequent planar slip have been reported by Oda *et al.*[1] There also exists another source of cyclic softening which is attributed to the gradual transition from random or crude dislocation cell structure to a clean cell structure.[19] This is observed to be particularly true for low nitrogen content N07 steel, as shown in Figure 2(c) where elongated cells can be seen. However, with increase in nitrogen content (>0.11 wt pct), the tendency to cell structure formation decreased (except near grain boundaries), and propensity to planar slip is manifested in the form of planar arrays of dislocations in N14 and N22 steels (as shown in Figure 2(d) for N22 steel), thus, contributing to the cyclic softening in later steels. Hence, enhanced cyclic softening in N14 and N22 steels could be explicitly attributed to the presence of SROs that promote planar slip. Reduction in SFE with nitrogen addition, though promotes planar slip, plays a minor role in promoting cyclic softening. This is because decrease in SFE, in general, contributes to the increase in strain-hardening rate, and accordingly, N22 should show low amount of cyclic softening in comparison to that of N07 steel. This is, however, in contrast to what is observed in the present study (Figures 2(a) and (b)).

2. *Dynamic strain aging and secondary cyclic hardening*

DSA and SCH are noticed in the investigated temperature range 773 K to 873 K (500 °C to 600 °C), although they showed strong dependence on applied strain amplitude. The above phenomena are found to increase the matrix strength, for the reasons discussed in the subsequent sections. Hence, at high temperatures,

partial/complete offset to cyclic softening is observed (Figures 3(a) and (b)) in comparison to that of 300 K (27 °C) (Figure 2(a)). Figure 2(b) also illustrates this, where the amount of cyclic softening incurred at 773 K (500 °C) is much less than at 300 K (27 °C), for all the steels. Effect of SFE at high temperatures could be negligible, as SFE of FeCrNi steels is found to increase with increase in temperature.[20] From the above observations, it can be deduced that in the investigated temperature range 773 K to 873 K (500 °C to 600 °C), DSA and SCH influence the cyclic deformation behavior over and above that controlled by interstitial nitrogen and SROs. Therefore, the influence of DSA and SCH on cyclic deformation is discussed in-detail in the following sections, as a function of temperature, strain amplitude, and nitrogen, along with deformation substructures.

a. Dynamic strain aging. DSA fundamentally results from attractive interaction between solute species and mobile dislocations, either during their glide[21] or temporary arrest at local obstacles in the glide plane.[22] Consequently, in order to maintain an imposed strain rate, an increase in flow stress is mandatory either to unlock the dislocations from obstacles or to generate new dislocations. DSA being an attractive interaction between the solute atoms and dislocations, its occurrence depends on the balance between the velocity of dislocations and diffusivity of the solute atoms (responsible for DSA). This in turn depends principally on the applied strain rate and test temperature, respectively; usually an increase in strain rate increases the dislocation velocity (at a constant dislocation density), and an increase in temperature increases the diffusivity of solute atoms. Thus, a decrease in strain rate at low temperatures or an increase in strain rate at high temperatures is mandatory to establish the balance between dislocation mobility and diffusion of solute atoms (to pin the dislocations). This makes DSA, a time and temperature-dependent phenomenon, and thus flow stress increases with decrease in strain rate or increase in temperature. Hence, an anomalous stress response, *i.e.*, increase in stress with increase in temperature, is observed in the temperature regime 773 K to 873 K (500 °C to 600 °C), indicating the occurrence of DSA as shown in Figures 3(a) and (b) at 0.4 and 0.6 pct strain amplitude for N14 steel. A similar result is observed for other nitrogen variations in 316LN SS. To emphasize the hardening resulting during DSA, the amount of initial cyclic hardening at 773 K and 300 K (500 °C and 27 °C) is plotted in Figure 3(c) at +0.6 pct strain amplitude; the amount of hardening is calculated as the difference between the peak stress and first cycle stress. Considerable matrix hardening during DSA occurrence at 773 K (500 °C) can be noticed, at all the nitrogen contents, in comparison to that at 300 K (27 °C) where DSA is absent. It is important to note that such high matrix hardening can result in substantial stress concentration at the crack tip that could accentuate rapid crack propagation and severe reduction in life.[4] The test temperature range 773 K to 873 K (500 °C to 600 °C), in the present study, coincides with the temperature range [673 K to 873 K (400 °C to 600 °C)] corresponding to the occurrence of DSA in 316LN SS.[3,4,23] In addition to the negative temperature dependence of CSR (Figures 3(a) and (b)), serrations are observed in the plastic portion of stress–strain hysteresis loops at all the strain amplitudes, irrespective of the nitrogen content. Serrations are shown in Figures 4(a) and (b) for N07 and N22 steel at 873 K and 823 K (600 °C and 550 °C), respectively, at 2nd cycle and at a cycle number corresponding to half-life. However, with continued cycling, decrease in magnitude of stress drop associated with serrations and also the decrease in density of serrations are observed, as shown in Figures 4(a) and (b) at half-life cycle. The decrease is found to be significant for strain amplitudes >0.6 pct. Most of the serrations are found to be of Type-B or C or a combination of them.

Dislocation-solute interactions during DSA restrict the cross slip of dislocations and increase the tendency toward planar mode of deformation, in addition to that caused by nitrogen. But the slip mode of deformation is, however, found to change with nitrogen content and applied strain amplitude. For instance, at 0.4 pct strain amplitude, planar slip bands are noticed in 316LN SS with nitrogen content above 0.07 wt pct at 823 K and 773 K (550 °C and 500 °C) [shown in Figures 3(d) and (e) for N14 and N22 steels at 823 K (550 °C)], in comparison to homogenous deformation in N07 steel (Figure 3f). Similarly at 0.6 pct amplitude, only slip bands are seen in N22 steel (Figure 4c), and with further decrease in nitrogen content ≤0.14 pct, tendency toward wavy/mixed slip mode of deformation is noticed. This transition is clearly evidenced through the formation of dislocation wall structures (in addition to slip bands) in N14 (Figure 4d) and cell structures in N07 (Figure 4e) steels, even though inverse temperature dependence of CSR similar to that in Figure 3(b) is observed. In 316 type austenitic stainless steel, solute atoms responsible for DSA are identified to be interstitial carbon and/or nitrogen atoms at low temperatures [<623 K (350 °C)] and substitutional Cr-atoms at high temperatures [673 K to 923 K (400 °C to 650 °C)].[24–26]

Further increase in strain amplitude to 0.8 or 1.0 pct is found to suppress the occurrence of DSA and cause diminishing of 'inverse temperature dependence' and hence DSA. Thus, CSR is observed to decrease with increase in temperature as shown in Figures 5(a) and (b) where CSR at 823 K and 873 K (550 °C and 600 °C) remained below (or close) to that of 773 K (500 °C), in all the steels. This signifies the fact that planar slip due to DSA can be suppressed by the increase in tendency toward multiple slip, which is intrinsic at high strain amplitude cycling. This can also be noticed from the decrease in stress drop in a serration and density of serrations at half-life cycle (Figures 4(a) and (b)). During DSA, to maintain an imposed strain rate, increase in mobile dislocation density is mandatory and is achieved either by unlocking of pinned dislocation or by generation of new dislocations. At the same time, application of high cyclic strain amplitudes, for

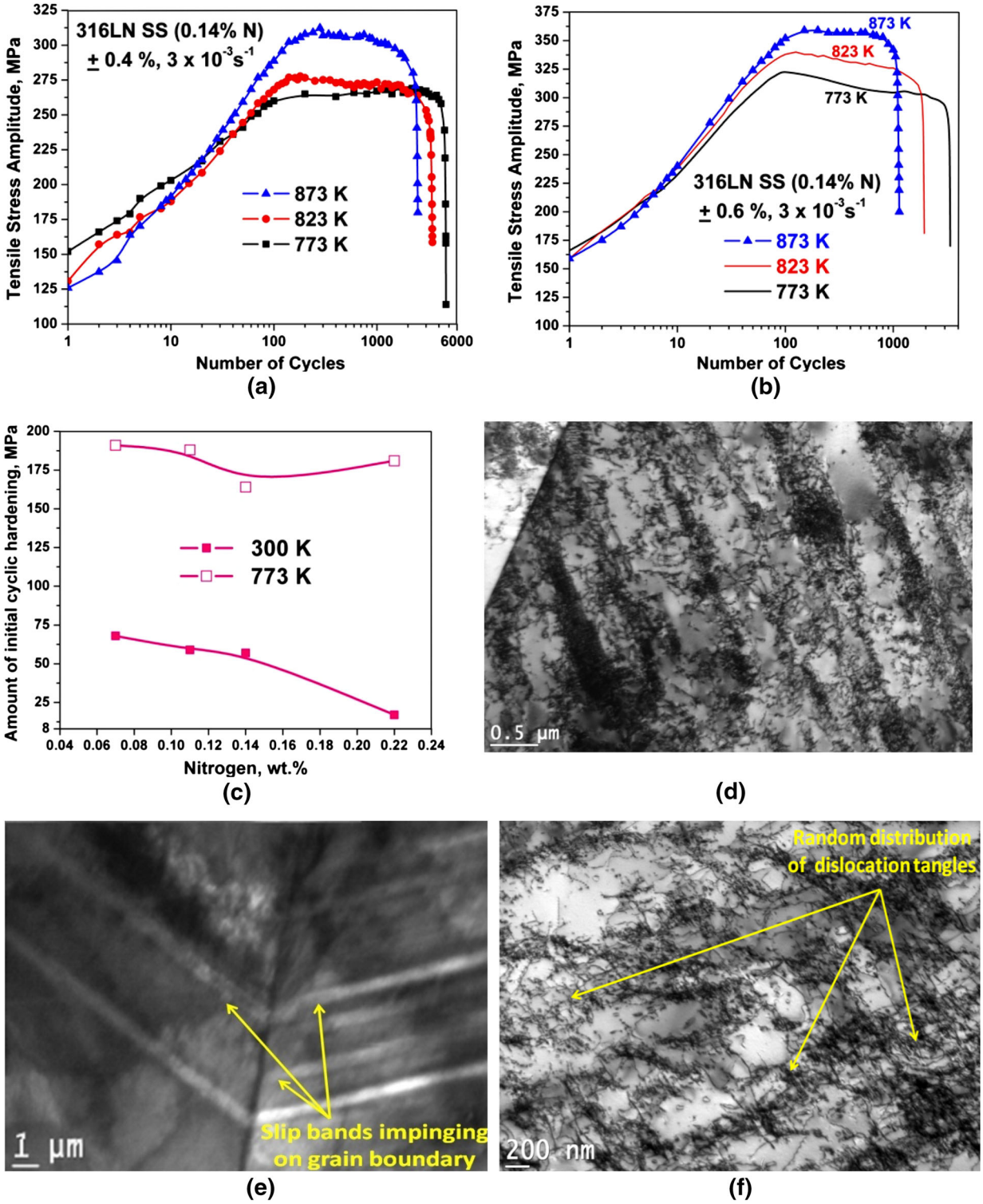

Fig. 3—(*a*, *b*) Inverse temperature dependence of cyclic stress response (CSR) in the temperature range of 773 K to 873 K (500 °C to 600 °C) in N14 steel at, (a) 0.4 pct strain amplitude, (b) 0.6 pct strain amplitude, and (*c*) Comparison of amount of initial hardening; (*d* through *f*) Deformation substructures [at 823 K (600 °C), 0.4 pct], illustrating planar mode of deformation in (d) N14 steel, (e) N22 steel, and (f) wavy mode of deformation in N07 steel.

e.g., 0.8 and 1.0 pct as in the present case, partially fulfills the need to generate mobile dislocations (during DSA) by activation of multiple slip systems and cross slip. This therefore suggests that, at high strain amplitudes, though cyclic deformation is accompanied by DSA, high dislocation activity inherent at high strain amplitudes also accomplishes the imposed strain rate. This, in addition to the dislocation–dislocation

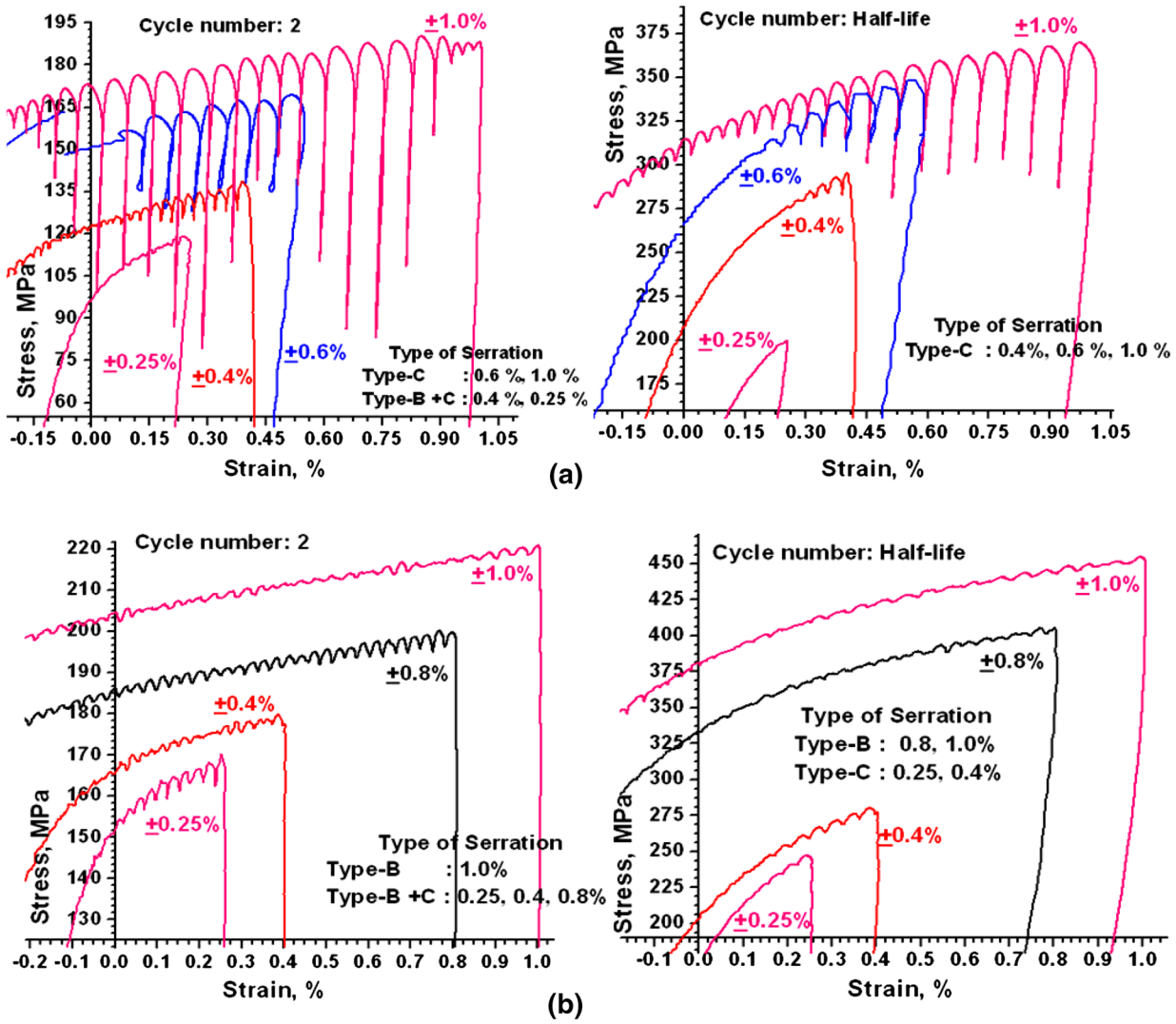

Fig. 4—(*a*, *b*): Serrations in tensile portion of hysteresis loop of 2nd cycle and half-life cycle, at various strain amplitudes, in (a) N07 steel, 873 K (600 °C) and (b) N22 steel, 823 K (550 °C); (*c* through *e*): Substructures at 823 K (550 °C) and 0.6 pct amplitude, illustrating transition from planar to wavy mode of deformation with decreasing nitrogen content, (c) slip bands in N22 steel, (d) dislocation cells forming from the wall structures in N14 steel and (e) elongated cells developed from wall structures in N07 steel.

interactions, could cause the above observed decrease in stress drop in a serration and density of serrations at high strain amplitudes. Thus, the manifestations of DSA diminish at high strain amplitudes >0.6 pct and hence cause positive temperature dependence of CSR as shown in Figures 5(a) and (b). Also, simultaneous occurrence of thermally activated dislocation motion (by cross slip and climb) could further contribute to the decrease in CSR with the increasing temperature at high strain amplitudes due to high dislocation activity. Accordingly, at high strain amplitudes (of 0.8 or 1.0 pct), deformation substructures revealed development of dislocation cell or wall structures depending on the nitrogen content (Figures 5(c) through (f)), cells being predominant in N07 and N11 steels. No evidence of planar arrays of dislocations is noticed at 0.8 or 1.0 pct strain amplitudes. At 0.25 pct strain amplitude, DSA is found to be absent or nominal in all nitrogen levels at 873 K (600 °C); the absence of serrations in half-life hysteresis loop can be noticed at 873 K (600 °C)/ 0.25 pct in Figure 4(a). But at this amplitude, cyclic deformation is noticed to be influenced predominantly by SCH as discussed in the subsequent section.

It is intuitive to anticipate the cyclic strain-induced precipitation, as temperatures in the present study are sufficiently high. It has been reported that precipitation of carbides ($M_{23}C_6$ and M_6C) in 316L SS required about 50 hours at 873 K (600 °C).[27] Also, nitrogen addition to 316L SS is reported to delay the onset of carbide precipitation.[15,16,28] In contrast to these observations, $M_{23}C_6$ carbide precipitates are observed in the present study irrespective of nitrogen content, but at 873 K (600 °C) only that too at strain amplitudes ≥0.6 pct, as shown in Figures 6(a) and (b) for N07 and N22 steel at 873 K (600 °C). Diffraction analysis of the precipitates is also shown in Figures 6(a) and (b). Thus, at 873 K

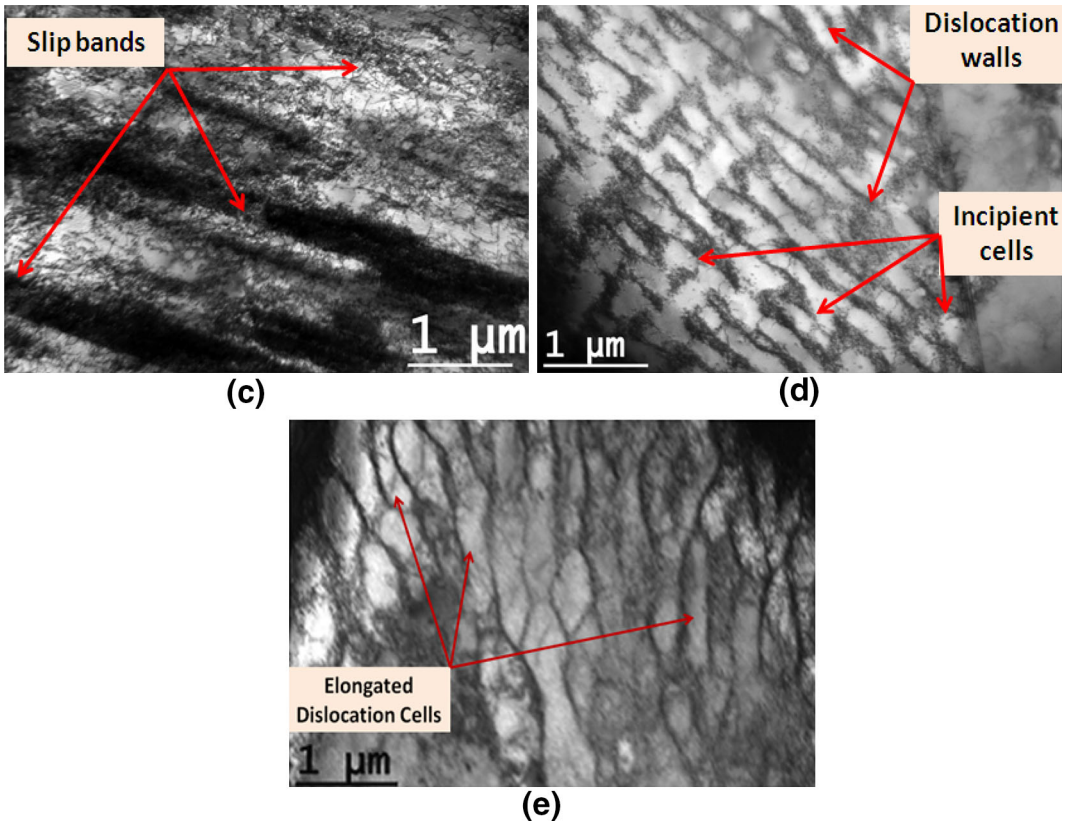

Fig. 4—continued.

(600 °C), in addition to DSA, these precipitates also contribute to matrix hardening. Precipitation of chromium carbides and nitrides is reported in LCF tested nitrogen-alloyed 316L SS, but in low strain rate ($<3 \times 10^{-4}$ s^{-1}) tests at 823 K and 873 K (550 °C and 600 °C).[29]

b. Secondary cyclic hardening. SCH is the hardening observed in CSR curves after brief stabilization, as shown in Figure 7(a) where secondary hardening can be seen up to rapid stress drop concomitant with macrocrack propagation. Since SCH introduces additional hardening, and as it occurs concurrently with DSA, it can have marked influence on fatigue life. Tests conducted at low strain amplitudes (±0.25, ±0.4 pct) revealed SCH at 773 K (500 °C). As apparent from Figure 7(a), tendency to SCH and the amount of hardening incurred during SCH increased with increase in nitrogen content. However, SCH is observed to diminish or disappear with increase in temperature or strain amplitude or both (Figure 7(b)), particularly for N contents ≤0.11 wt pct N. For strain amplitudes ≥0.6 pct, SCH completely vanished (Figures 3(b) and 5(a) and (b)).

Increase in degree of hardening during SCH can be presumed to result from either cyclic strain-induced precipitation or formation of particular dislocation structure. Occurrence of SCH has been attributed to deformation-induced martensitic transformation at room temperature in 316L SS.[30] It is also reported that SCH results from formation of corduroy structure (alternate empty channels and black bands consisting of small dislocation loops, debris, and cavities) at 473 K to 673 K (200 °C to 400 °C) in 316L type stainless steels[5] and cell structure refinement in interstitial free steel.[31] To analyze the cause for SCH, interrupted tests were conducted at various stages during SCH period.[32] Deformation substructures essentially revealed planar mode of deformation, *i.e.*, planar slip bands (Figures 7(c) through (e)) containing planar arrays of dislocations dispersed with constituents such as dipoles, multipoles, small dislocation loops, and dislocation pairs (Figure 7(f)). These constituents increased with increase in nitrogen content, possibly due to increase in slip planarity with nitrogen. These constituents act as strong obstacles to the dislocation motion, and particularly dipoles and multipoles are reported to cause linear hardening.[33] In addition, decrease in interband spacing (Figures 7(c) through (e)) during SCH reduces the effective mean free path of mobile dislocations, thus further adding to the stress increase during secondary hardening. Hence, the hardening during SCH is attributed to the above observations.

From the Sections III–A–1 and III–A–2, it is important to point out that, the source for the origin of planar mode of deformation is found to determine the consequences of planar slip and associated hardening/softening behavior. At 300 K (27 °C) and 0.6 pct amplitude, planar mode of deformation is evidenced in the substructures of 316LN SS with 0.14 and 0.22 wt pct N, as

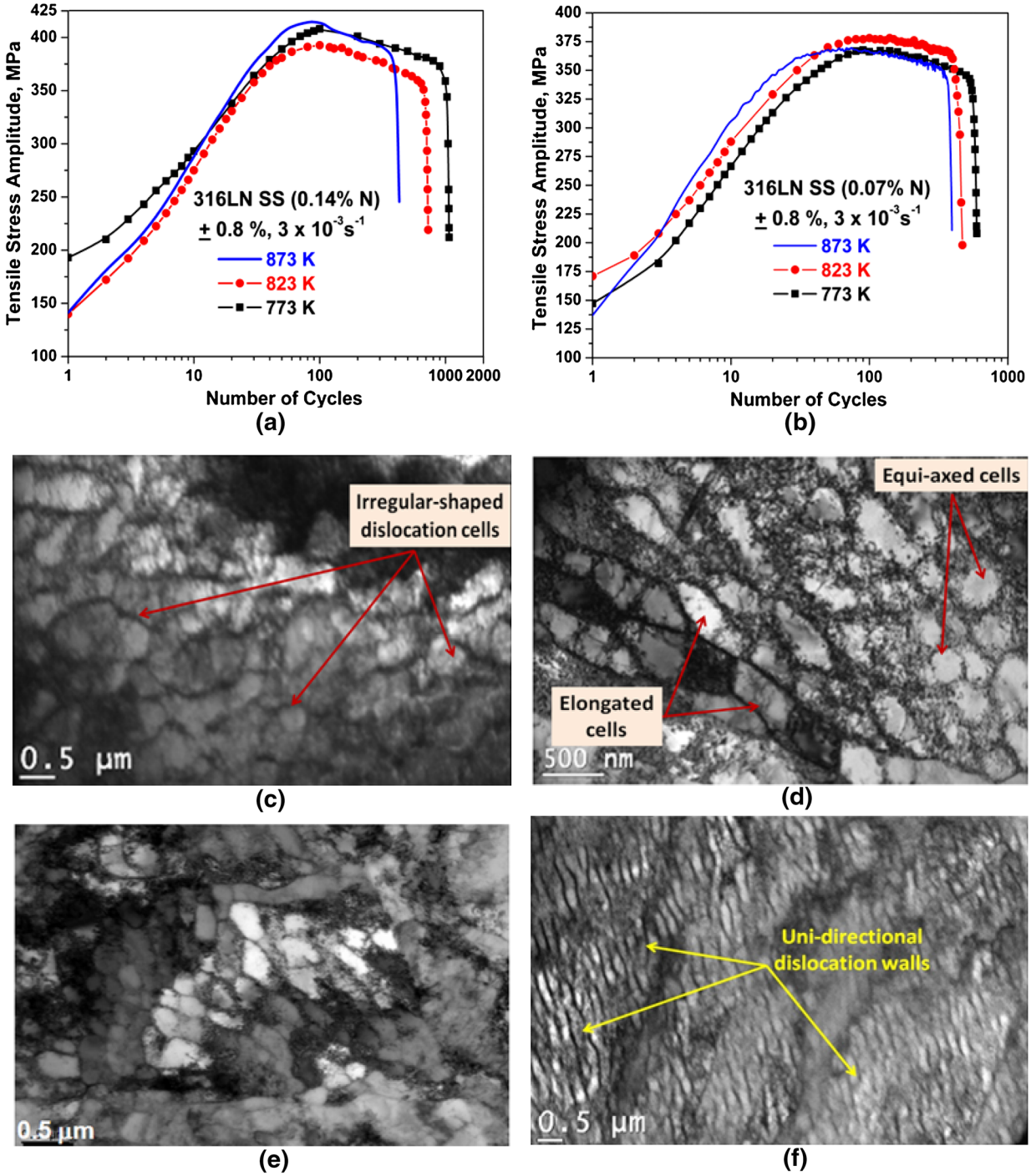

Fig. 5—Influence of high strain amplitude (0.8 pct) on cyclic stress response curves in (*a*) N14 steel, (*b*) N07 steel; (*c* through *f*) Development of deformation substructure at 823 K (550 °C) and 1.0 pct strain amplitude in (c) N07, (d) N11, (e) N14, and (f) N22 steel.

shown in Figure 2(d) for N22 steel. In this case, the origin of planar slip is essentially due to the slip localization phenomenon as revealed by the coplanar accumulation of dislocations in the form of closely packed dislocation arrays (Figure 2(d)). In austenitic stainless steels, such slip localization is reported to arise from the disordering of Cr-N SROs by passage of first few dislocations that provide easy path for subsequent dislocation motion.[1] This is found to manifest in the form of pronounced cyclic softening in the CSR curves (in N14 and N22 steels) as apparent from Figure 2(a), and also the amount of softening is found to increase with increasing nitrogen content (Figure 2(b)). In contrast to the above, at high temperatures [773 K to 873 K (500 °C to 600 °C)], planar mode of deformation is evidenced in the form of planar slip bands (*e.g.*, Figures 3(d) and (e) and 7(c) through (e)) and is found to cause considerable matrix hardening, particularly for

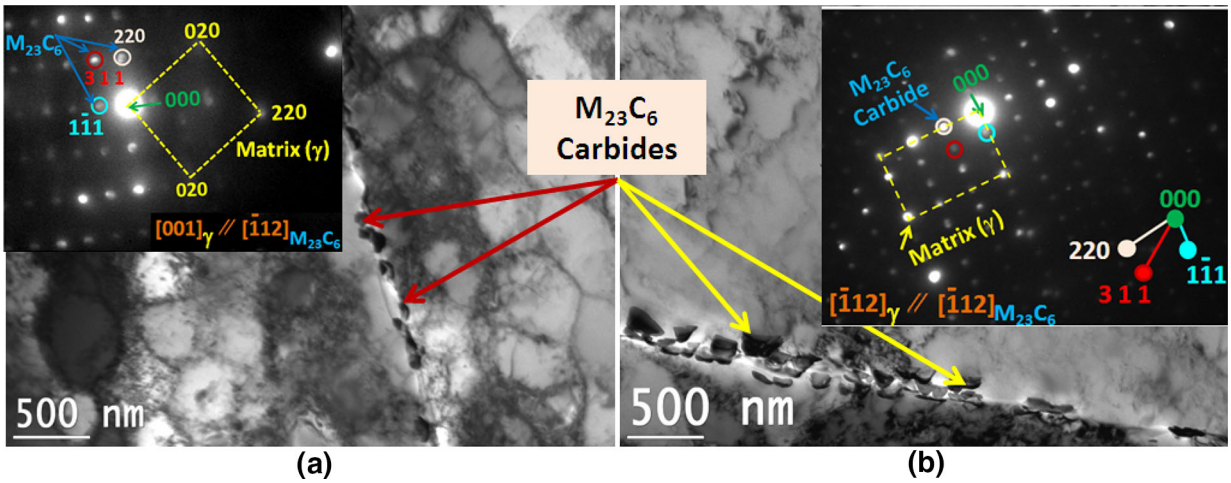

Fig. 6—Cyclic strain-induced precipitation of $M_{23}C_6$ carbides at grain boundaries during LCF testing at 873 K (600 °C) and 0.6 pct strain amplitude, in (*a*) N07 steel and (*b*) N22 steel; inset shows diffraction pattern from carbide along with matrix (γ) and orientation relationship between them; in case of (a), precipitate zone axis [−112] is close to (2 to 3 deg away) that of matrix [001].

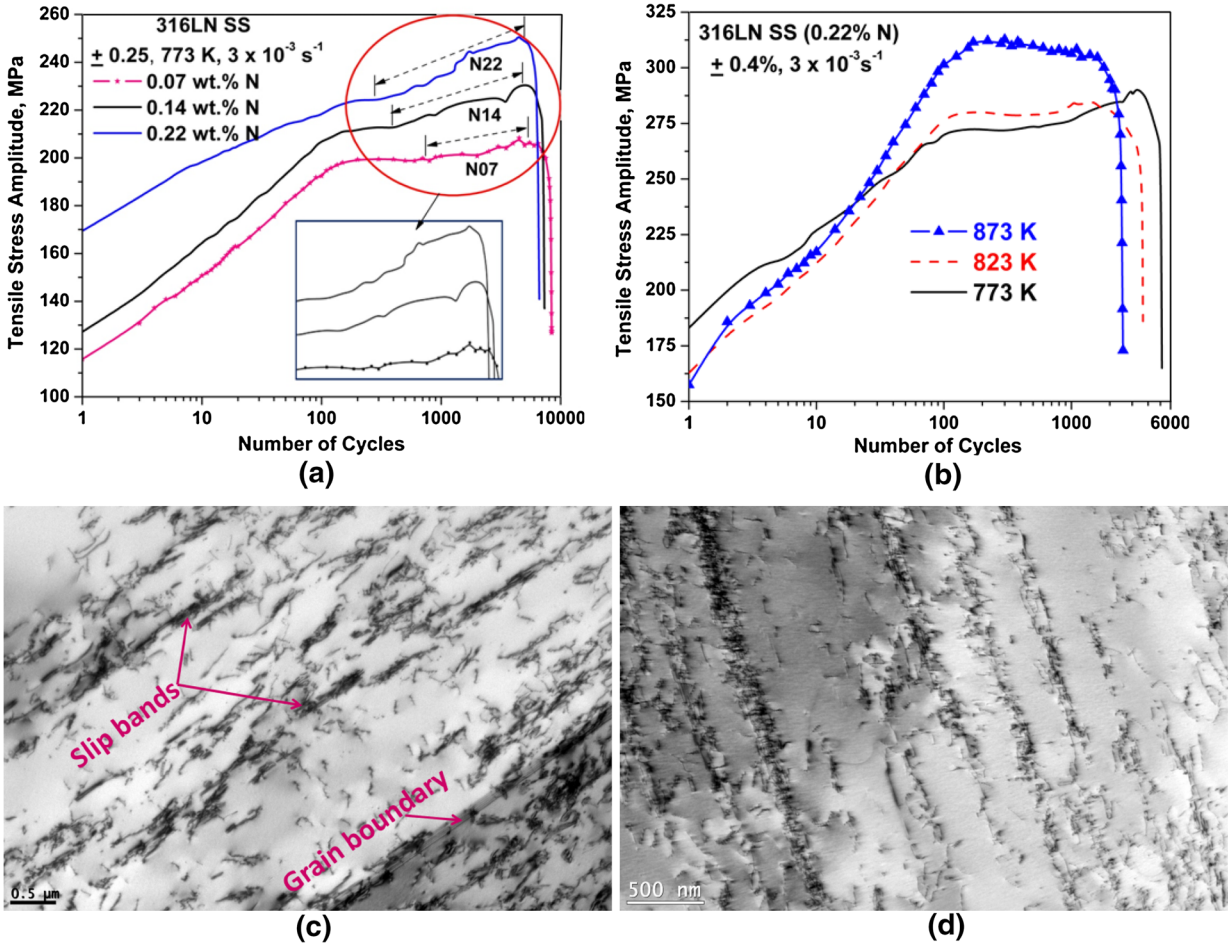

Fig. 7—(*a*, *b*) Influence of nitrogen content and temperature on occurrence of SCH in 316LN SS at 0.25 and 0.4 pct strain amplitude, respectively, and (*c* through *e*) Deformation substructures developed during SCH, in (c) N14 steel after start of SCH (N = 1460 cycles), (d) N14 steel at middle of SCH (N = 3500), (e) N14 steel after SCH period (N = 7208), (*f*) magnified view of the slip bands taken at the middle of SCH in N22 and N14 steel, revealing dislocation dipoles (D), multipoles (M), dislocation pairs (C), and small dislocation loops; test condition for Figs. 7(c) through (e) is the same [773 K (500 °C), ±0.25 pct), and the corresponding CSR curve for N14 steel is shown in (a)[32].

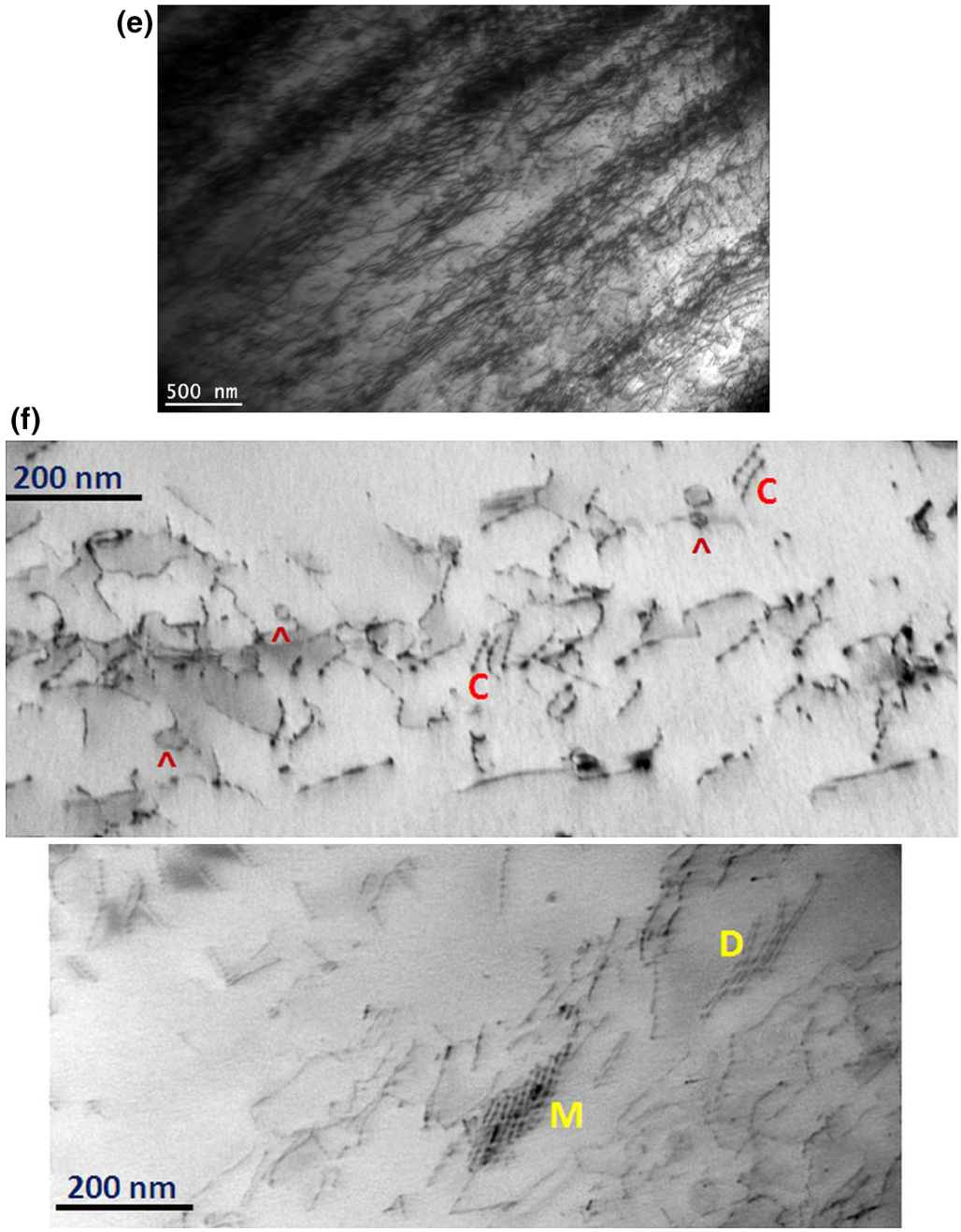

Fig. 7—continued.

strain amplitudes < 0.6 pct (as shown in CSR curves, Figures 3(a) and 7(a) and (b)). It is apparent from figures that, CSR curves portrayed pronounced initial cyclic hardening followed with cyclic saturation and/or secondary hardening, rather than cyclic softening. The origin of planar slip that caused the development of slip bands is attributed to result from the occurrence of DSA and SCH. Both DSA and SCH are found to offset the cyclic softening and enhance matrix hardening, at high temperatures, for the reasons mentioned in Sections III–A–2–a and III–A–2–b. It is therefore important to mention that planar mode of deformation can alter the CSR behavior from cyclic softening to cyclic hardening depending on the test temperature, strain amplitude, and nitrogen content.

B. *Cyclic Stress–Strain Curves (CSSCs)*

Cyclic stress–strain curves shown in Figures 8(a) and (b) are log–log scale plots of half-life tensile stress amplitude *vs* half-life plastic strain amplitude, for N07, N11, N14, and N22 steels, at 773 K and 873 K (500 °C and 600 °C). At 773 K (500 °C), nearly linear CSSC is observed with a single slope over the entire range of tested strain amplitudes, while a dual-slope linear CSSC is noticed at 873 K (600 °C) with a transition in slope at

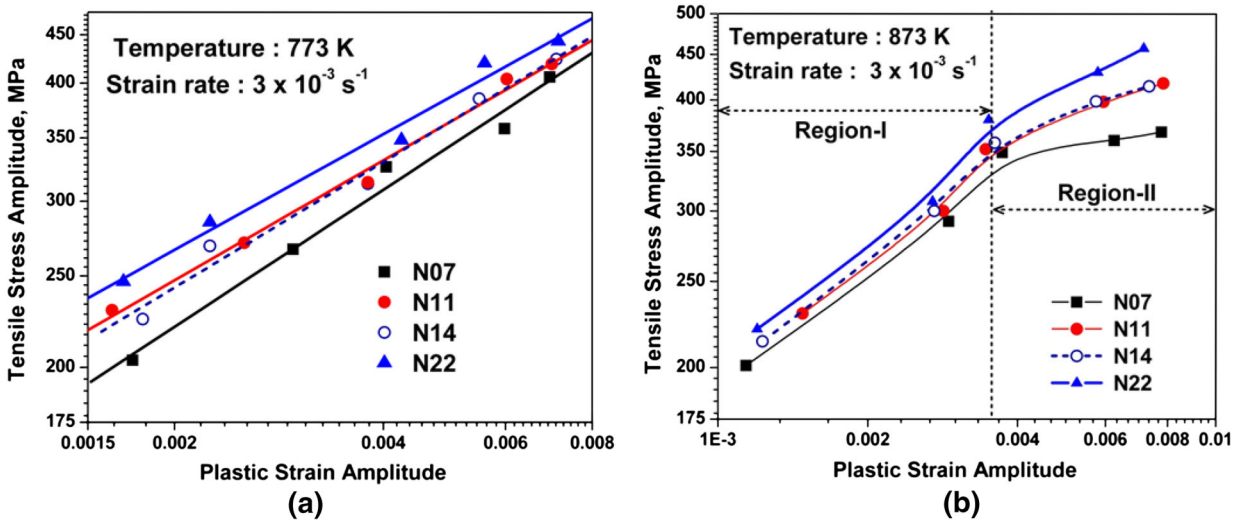

Fig. 8—Cyclic stress strain curves (in log–log scale) for N07, N11, N14, and N22 steels at (*a*) 773 K (500 °C) and (*b*) 873 K (600 °C).

Table II. Cyclic Strain-Hardening Exponent (n') and Cyclic Strength Coefficient (K', in MPa) Values of 316LN SS with Varying Nitrogen Content, at 773 K and 873 K (500 °C and 600 °C)

	773 K (500 °C)		873 K (600 °C)			
			n'		K'	
Designation	n'	K'	Region-I	Region-II	Region-I	Region-II
N07	0.482	4408	0.447	0.069	4134	515
N11	0.422	3413	0.478	0.210	5161	1160
N14	0.442	3778	0.467	0.208	4872	1157
N22	0.407	3340	0.483	0.254	5611	1601

about 0.355 pct plastic strain amplitude (corresponding to the 0.6 pct applied total strain amplitude). The different slopes in region-I and II (see Figure 8(b)) at 873 K (600 °C) indicate the differences in nature of strengthening contributions and associated cyclic strain hardening in respective regions. To gain further insight into this discrepancy at 873 K (600 °C), cyclic strain-hardening exponent (n') and cyclic strength coefficient (K') are obtained from the log–log scale plots of CSSCs (shown in Figures 8(a) and (b)) as per the power law equation:

$$\frac{\Delta\sigma}{2} = K'\left(\frac{\Delta\varepsilon_p}{2}\right)^{n'}, \qquad [1]$$

where $\Delta\sigma/2$ is half-life tensile stress amplitude, and $\Delta\varepsilon_p/2$ is plastic strain amplitude. Table II lists the values of n' and K' as a function of nitrogen content at 773 K and 873 K (500 °C and 600 °C) (for regions I and II). Interestingly, region-I has shown significantly high n' and K' values compared to those of in region-II. This is in agreement with the observations in Section III–A–2 which signify that DSA and SCH enhance the CSR particularly at total strain amplitudes ≤0.6 pct (region-I), compared to cyclic straining at high strain amplitudes (region-II) where DSA/SCH effects are negligible/absent. Hence, high n' (slope) in region-I is because of DSA and/or SCH which contributes to matrix hardening significantly, in addition to the intrinsic strength, whereas in region-II, their contribution decreases, as SCH completely vanishes and DSA being suppressed by cross slip and multiple slip that could be more significant at temperatures higher than 773 K (500 °C). Furthermore, intergranular precipitation [at 873 K (600 °C), Figure 6] in region-II that can accompany removal of substitutional and interstitial elements from the matrix could also add to the decrease in n' value in region-II.

IV. SUMMARY

(a) Cyclic deformation of nitrogen-alloyed 316LN SS shows characteristic cyclic softening (after brief initial hardening) at 300 K (27 °C), particularly for nitrogen contents >0.11 wt pct. At test temperatures 773 K to 873 K (500 °C to 600 °C), DSA and SCH are observed to offset the cyclic softening partially/completely.

(b) SCH and DSA are observed to result from planar mode of deformation, and their occurrence is found to be dependent on applied strain amplitude. DSA is observed up to ±0.6 pct total strain amplitude beyond which DSA is noticed to be negligible. SCH is evidenced only for strain

amplitudes of 0.25 and 0.4 pct. Tendency to SCH decreased with the increasing temperature and with the decreasing nitrogen content.

(c) At 0.07 wt pct N, dislocation cell structures are predominantly observed over the entire range of strain amplitudes, except at 0.25 pct. For other nitrogen contents in 316LN SS, deformation mode is observed to be planar, wavy, or mixed mode depending on nitrogen content and applied strain amplitude.

(d) 316LN stainless steel, at all nitrogen contents, exhibited linear relationship in cyclic stress-strain curves (plotted in log–log scale) over the entire range of applied strain amplitudes at 773 K (500 °C), whereas bi-linear curves are observed at 873 K (600 °C).

ACKNOWLEDGMENTS

The authors would like to thank Mr. P. Shyamala Rao, IGCAR, Kalpakkam for providing SEM facility and Mr. Srinivasa Rao (IGCAR) and Mrs. Kanchanamala, Mr. Papa Rao, IIT Madras for assistance in TEM sample preparation and examination.

REFERENCES

1. K. Oda, N. Kondo, and K. Shibata: *ISIJ Int*., 1990, vol. 30 (8), pp. 625–31.
2. I. Karaman, H. Sehitoglu, H.J. Maier, and Y.I. Chumlyakov: *Acta Mater*., 2001, vol. 49, pp. 3919–33.
3. A.F. Armas, O.R. Bettin, I. Alvarez-Armas, and G.H. Rubiolo: *J. Nucl. Mater*., 1988, vols. 155–157, pp. 646–49.
4. G.V. Prasad Reddy, R. Sandhya, K.B.S. Rao, and S. Sankaran: *Proc. Eng*., 2010, vol. 2, pp. 2181–88.
5. M. Gerland, R. Alain, B. Ait Saadi, and J. Mendez: *Mater. Sci. Eng. A*, 1997, vol. 229, pp. 68–86.
6. J.O. Nilsson: *Fatigue Eng. Mater. Struct*., 1984, vol. 7 (1), pp. 55–64.
7. S. Degallaix, J. Foct, and A. Hendry: *Mater. Sci. Technol*., 1986, vol. 2, pp. 946–50.
8. R. Taillard and J. Foct: *Proc. Int. Conf. on High Nitrogen Steels*, HNS'88, Lille, France, 1989, pp. 163–68.
9. S. Degallaix, G. Degallaix, and J. Foct: in *Low Cycle Fatigue, ASTM STP 942*, H.D. Solomon, G.R. Halford, L.R. Kaisand, and B.N. Leis, eds., ASTM, Philadelphia, 1988, pp. 798–811.
10. D.W. Kim, W.-S. Ryu, J.H. Hong, and S.-K. Choi: *J. Nucl. Mater*., 1998, vol. 254, pp. 226–33.
11. G.V. Prasad Reddy, R. Sandhya, M.D. Mathew, and S. Sankaran: *Metall. Mater. Trans A*, 2014, in press.
12. V.G. Gavriljuk and H. Berns: *High Nitrogen Steels: Structure, Properties, Manufacture, Applications*, 1st ed., Springer Verlag, Berlin, 1999.
13. X.W. Zhou and M. Grujicic: *CALPHAD*, 1996, vol. 20 (3), pp. 257–72.
14. Yu. Jagodzinski, S. Smouk, A. Tarasenko, and H. Hänninen: *Mater. Sci. Forum*, 1999, vols. 318–320, pp. 309–14.
15. M.D. Mathew, K. Laha, and V. Ganesan: *Mater. Sci. Eng. A*, 2012, vol. 535, pp. 76–83.
16. G. Wahlberg, U. Rolander, and H.O. Andren: *Proc. Int. Conf. on High Nitrogen Steels*, HNS'88, Lille, France, 1989, pp. 163–68.
17. M. Murayama, K. Hono, H. Hirukawa, T. Ohmura, and S. Matsuoka: *Scripta Mater*., 1999, vol. 41 (5), pp. 467–73.
18. V.V. Sumin, G. Chimid, T. Rashev, and L. Saryivanov: *Mater. Sci. Forum*, 1999, vols. 318–320, pp. 31–40.
19. A.P.L. Turner: *Metall. Trans. A*, 1979, vol. 10A, pp. 225–34.
20. L. Remy and A. Pineau: *Mater. Sci. Eng*., 1978, vol. 36, pp. 47–63.
21. A.H. Cottrell: *Dislocations and Plastic Flow in Crystals*, Oxford University, London, 1953.
22. A.W. Sleeswyk: *Acta Metall*., 1958, vol. 6 (9), pp. 598–603.
23. G.V. Prasad Reddy, R. Sandhya, M. Valsan, and K.B.S. Rao: *Mater. Sci. Technol*., 2010, vol. 26 (11), pp. 1384–92.
24. C.F. Jenkins and G.V. Smith: *Trans. Metall. Soc. AIME*, 1969, vol. 245, pp. 2149–56.
25. K.G. Samuel, S.L. Mannan, and P. Rodriguez: *Acta Metall*., 1988, vol. 36 (8), pp. 2323–27.
26. S.-G. Hong and S.-B. Lee: *J Nucl. Mater*., 2005, vol. 340 (2–3), pp. 307–14.
27. D. Pecker and I.M. Bernstein: *Handbook of Stainless Steels*, McGraw-Hill, New York, 1977.
28. B.S. Rho and S.W. Nam: *J. Nucl. Mater*., 2002, vol. 300, pp. 65–72.
29. V.S. Srinivasan, M. Valsan, R. Sandhya, K.B.S. Rao, S.L. Mannan, and D.H. Sastry: *Int. J. Fat*., 1999, vol. 21, pp. 11–21.
30. J. Man, K. Obrtlík, M. Petrenec, P. Beran, M. Smaga, A. Weidner, J. Dluhoš, T. Kruml, H. Biermann, D. Eifler, and J. Polák: *Proc. Eng*., 2011, vol. 10, pp. 1279–84.
31. C.-C. Shiha, N.-J. Hoa, and H.-L. Huangb: *Mater. Charact*., 2009, vol. 60, pp. 1280–88.
32. G.V. Prasad Reddy, R. Sandhya, M.D. Mathew, and S. Sankaran: *Metall. Mater. Trans. A*, 2013, vol. 44A, pp. 5625–29.
33. H.S. Chen, J.J. Gilman, and A.K. Head: *J. Appl. Phys*., 1964, vol. 35 (8), pp. 2502–14.